Talanta 132 (2015) 658–663

Contents lists available at ScienceDirect

Talanta

journal homepage: www.elsevier.com/locate/talanta

# A novel biosensor based on single-layer $MoS_2$ nanosheets for detection of $Ag^+$

Kang Mao, Zitong Wu, Yinran Chen, Xiaodong Zhou *, Aiguo Shen, Jiming Hu

*Key Laboratory of Analytical Chemistry for Biology and Medicine (Ministry of Education), College of Chemistry and Molecular Sciences, Wuhan University, Wuhan 430072, China*

ARTICLE INFO

*Article history:*
Received 24 July 2014
Received in revised form
10 October 2014
Accepted 13 October 2014
Available online 22 October 2014

*Keywords:*
Single layer $MoS_2$
$Ag^+$
"C–$Ag^+$–C"
Fluorescence detection

ABSTRACT

In this work, we use for the first time single layer $MoS_2$ as the fluorescence quencher to design a detection method for $Ag^+$ with excellent robustness, selectivity and sensitivity. To maintain the ultrathin $MoS_2$, bulk $MoS_2$ materials have been exfoliated by intercalation with lithium followed by reaction with water. As-prepared two-dimensional $MoS_2$ not only has good water-solubility but also obtains high fluorescence quenching efficiency within 5 min. Importantly, the detection limit of this assay for $Ag^+$ (1 nM) was lower than the maximum limitation guided by the United States Environmental Protection Agency (EPA) and the World Health Organization (WHO). Further, this new $Ag^+$ probe was demonstrated in monitoring $Ag^+$ in lake water samples with satisfactory results.



## 1. Introduction

As we all know, heavy metals are highly toxic and carcinogenic even at a trace level, which can enter the environment due to increasing industrial activities. They are non-biodegradable and can accumulate in the food chain, posing a severe threat to the environment and human health. Therefore, heavy metal pollution becomes a major concern for global sustainability. Among these heavy metal ions, silver ions ($Ag^+$) have received considerable attention in recent years because the use of silver, silver nanoparticles, and silver compounds has increased and recent studies emphasized bioaccumulation and the potential negative impact of $Ag^+$ on aquatic organisms [1–3]. Long term exposure of $Ag^+$ in water causes the death of exposed organisms such as environmentally benign bacteria [3]. Even nanomolar concentration of $Ag^+$ in water perturbs $Na^+$ and $Cl^-$ homeostasis of fishes and invertebrates [2]. It is therefore essential to monitor $Ag^+$ in the environment, drinking water, food and biological fluids.

Conventional methods for $Ag^+$ measurement include atomic absorption spectroscopy (AAS), inductively coupled plasma/mass spectrometry (ICP-MS), inductively coupled plasma/atomic emission spectrometry (ICP-AES), ultraviolet–visible (UV–vis) spectroscopy, etc. Although these techniques are highly sensitive and selective, they require tedious sample preparation and preconcentration procedures, expensive instruments, and professional personnel. Moreover, they are inappropriate to be used as portable devices for real-time and on-site detection. In contrast, biosensors, especially fluorescent sensing, have great potential in high throughput detection of $Ag^+$ on-site [4–7]. Further, rapid development of nanotechnology has provided new opportunities for improved performance of fluorescence sensors in terms of sensitivity, selectivity and reproducibility. Fluorescent sensing is based on analyte-induced changes in the physicochemical properties of fluorophores such as fluorescence intensity, lifetime, and anisotropy, which are related to charge transfer or energy transfer processes [8,9]. However, relatively a few fluorescent sensors for $Ag^+$ have been reported compared with fluorescent sensors for other metal ions [10–16]. Furthermore, most of the fluorescent sensors for $Ag^+$ showed limitations in practical application due to low water solubility or other drawbacks. Hence, it remains essential to develop much simple, efficient and robustness methods of silver ion probe that can be used for detection of $Ag^+$ in complex water samples.

The rise of graphene has recently inspired great research interest in other types of ultrathin nanomaterials due to their attractive properties and various potential applications [17,18]. Therefore, following the same vein on graphene study, researchers have started the exploration of graphene analogs materials comprising stacked atomic or molecular layers. Strong covalent bonds in layers and weak Van der Waals interaction between layers allow the graphene analogs to form a robust two-dimensional (2D) nanostructure. Layered molybdenum disulfide ($MoS_2$) is one of the typical graphene analogs and a prototypical transition metal dichalcogenide material, which consists of covalently bonded Mo and S atoms [19]. Single-layer $MoS_2$ can be viewed as an "S–Mo–S" [10] sandwich structure, stacking a positively charged molybdenum plane between two negatively charged sulfur planes. Every

* Corresponding author. Tel.: +86 27 68752439, +86 27 68758116.
*E-mail address:* zhouxd@whu.edu.cn (X. Zhou).

http://dx.doi.org/10.1016/j.talanta.2014.10.026
0039-9140/

Mo is coordinated in a trigonal prismatic geometry to six S atoms. Owing to the specific 2D confinement of electron motion and the absence of interlayer perturbation, the $MoS_2$ monolayer possesses a direct band gap, showing dramatic improvement in photoluminescence quantum efficiency [20–22] and leads to an attractive electrocatalytic activity [23].To our surprise, it has been found that some fluorescent dyes underwent drastic quenching in the presence of $MoS_2$ nanoparticles ($MoS_2$NCs). Zhu et al. [24] designed single-layer $MoS_2$ based nanoprobes which have been successfully used as a sensing platform for the detection of DNA and small molecules. Goswami et al. [25] reported that fluorescence of Hoechst 33258 was efficiently quenched in the presence of $MoS_2$ nanoparticles and estimated the probability of the distance distribution between the donor (Hoechst 33258) and acceptor ($MoS_2$NCs) by employing a statistical method based on Forster resonance energy transfer (FRET)-based model. Compared with other nano-materials, except high fluorescent quenching efficiency, cheap bulk $MoS_2$ materials are engineered easily and single layer $MoS_2$ has good water solubility. Such reports imply that single or fewer layers $MoS_2$ could also be one of the most valuable quenching materials in environmental, biomedical, and other applications.

Considering all of these mentioned above, to the best of our knowledge, we report for the first time a novel FRET-based method for $Ag^+$ based on single-layered $MoS_2$. It is known that oligonucleotides can interact with some types of metal ions with high specificity [26]. It has been previously demonstrated that $Ag^+$ can selectively bind in between two DNA cytosine (C) bases and promote these C–C mismatches to form stable C–$Ag^+$–C base pairs. The $Ag^+$-mediated C–$Ag^+$–C pairs are more stable and have higher melting temperature than the Watson–Crick C–G pairs. Further, $Ag^+$ can be incorporated into the DNA duplex without largely altering the double helical structure because the van der Waals radius of silver ($\approx$ 1.44 Å) is smaller than the base pair spacing of the DNA duplex ($\approx$ 3.4 Å) [27,28]. In this work, the excellent quenching performance of single layer $MoS_2$ was combined with $Ag^+$-mediated base pairs "C–$Ag^+$–C" to sensitively and selectively detect $Ag^+$. Scheme 1 shows the design of fabrication of the assay for $Ag^+$ on single layer $MoS_2$. Compared with other reported methods, the proposed method has some advantages of simple instrument, low background and high sensitivity both in aqueous buffer and complex water.

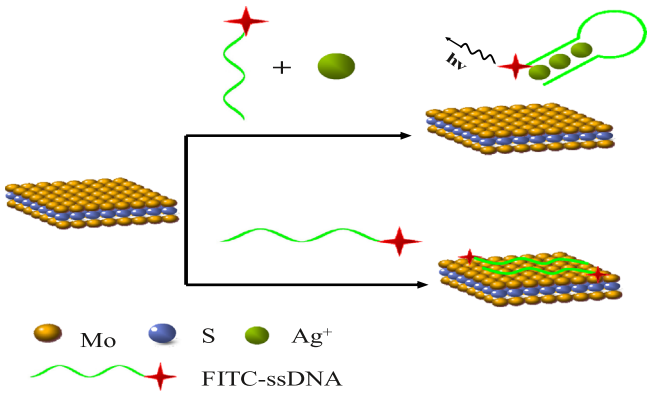


**Scheme 1.** Schematic representation of fluorescent detection of $Ag^+$ on single layer $MoS_2$ platform (a FITC-labeled $Ag^+$ specific oligonucleotide, rich in cytosine, is employed as the fluorescent probe in sensing targets. When FITC-labeled DNA probe is in the state of random coil ssDNA, FRET from FITC-ssDNA to single layer $MoS_2$ occurs and fluorescence disappears. However, when the DNA probe is in formation of dsDNA due to the addition of $Ag^+$, the energy donor FITC is far away from the surface of single layer $MoS_2$ and fluorescence will be recovered).

## 2. Materials and methods

### 2.1. Materials

(5′-FITC-CTCTCTTCTCTTCATTTTTCAACACAACACAC-3′) were purchased from Sangon Biotech (Shanghai, China) Co., Ltd. and purified by HPLC. Bulk $MoS_2$ and *n*-butyllithium were from Aladdin (Shanghai, China). $AgNO_3$ and other inspected species (including $Ni^{2+}$, $Cu^{2+}$, $Cr^{3+}$, $K^+$, $Na^+$, $Fe^{3+}$, $Pb^{2+}$, $Co^{2+}$, $Mn^{2+}$, $Hg^{2+}$, $Zn^{2+}$, $Al^{3+}$, $Fe^{2+}$, $Mg^{2+}$, $Cl^-$, $SO_4^{2-}$, $NO_3^-$ $HCO_3^-$ and $PO_4^{3-}$) were prepared with ultrapure water from a Millipore system (18.2 M resistivity). All the experiments were carried out in phosphate buffer saline (PBS) buffer (0.1 mM PBS, 50 mM $NaNO_3$, 10 μM EDTA [29], pH 8.00).

### 2.2. Instrumentation

Bulk $MoS_2$ material was characterized by a scanning electron microscope (SEM). The morphology of single layer $MoS_2$ was characterized by a JEM-2100 transmission electron microscope (TEM) operated at 200 kV. Subsequently, a confocal laser micro-Raman spectrometer (HR800UV, JOBIN YVON) was used to obtain the Raman spectra of single layer $MoS_2$ with excitation wavelength being set at 633 nm. Finally, a fluorescence spectrometer (F-4600, Hitachi Co. Ltd., Japan) with a Xenon lamp excitation source was employed to record fluorescence spectra. The excitation was set at 490 nm and the emission was monitored at 518 nm.

### 2.3. Preparation of single layer $MoS_2$

Single-molecular-layer $MoS_2$ was prepared by exfoliation of lithium-intercalated $MoS_2$ powder in water with some modifications [30–32]. 0.35 g of layered bulk $MoS_2$ materials were mixed with 100 mL 1 M of *n*-butyl lithium in hexane solution, then the mixtures were stirred and allowed to react in nitrogen environment for 48 h at room temperature. After the mixture was filtrated, washed with hexane several times and dried, the lithium-intercalated $MoS_2$ powder obtained was exfoliated under ultrasonication for over 0.5 h (120 W) in 100 mL ultrapure water. During the whole experimental process, the lithium ions fulfill several important functions. First, the Li ions are inserted into the interlayer space of the layered bulk $MoS_2$ material, which expands the interlayer distance and weakens the van der Waals interactions between the layers. Second, the inserted $Li^+$ ions are subsequently reduced to $Li^0$ by accepting electrons during the discharge process. The metallic lithium can react with water to form LiOH and produce hydrogen gas. The generated hydrogen gas pushes the layers further apart [33]. Finally, the obtained stable $MoS_2$ dispersion was centrifuged to remove the unexfoliated monolayer $MoS_2$ and get the homogeneous single layer $MoS_2$ suspension (1.0 mg/mL).

### 2.4. Fluorescence spectra measurements

#### 2.4.1. Selection of optimal $MoS_2$ concentration

FITC-ssDNA solution (500 nM) was incubated for 5 min at 90 °C and then cooled down slowly to the room temperature. Single layer $MoS_2$ solution was diluted by PBS buffer (pH 8.00) to a final concentration of 0.05 mg/mL. Different volumes (0–300 μL) of single layer $MoS_2$ solution (0.05 mg/mL) were mixed with 10 μL 500 nM of FITC-ssDNA in 1.5 mL test tube, and different volumes of PBS buffer were added to make each solution 400 μL, then these mixtures were vibrated and allowed to react for 0.5 h at 30 °C. Finally the fluorescence measurements were done at room temperature. To save the cost and time, kinetic assay is necessary to find turning point that fluorescence quenching and fluorescence recovery. 200 μL of single layer $MoS_2$ solution (0.5 mg/mL) was mixed with 10 μL 500 nM of FITC-ssDNA in cuvette, after 15 min,

20 μL of 2 μM $Ag^+$ in aqueous buffer and 170 μL PBS buffer were added. The fluorescence spectra were measured at 30 °C.

#### 2.4.2. Assay for $Ag^+$ in aqueous buffer

FITC-ssDNA solution (500 nM) was incubated for 5 min at 90 °C, then cooled down slowly to the room temperature. 200 μL of single layer $MoS_2$ solution (0.05 mg/mL) was mixed with 10 μL 500 nM of FITC-ssDNA in 1.5 mL test tube, then the mixed solution was stirred and allowed to react for 5 min at 30 °C, after that, different volumes of 2 μM $Ag^+$ in aqueous buffer (0–20 μL) were added; finally, appropriate aliquot of PBS buffer (pH 8.00) was introduced to make each reaction solution 400 μL and final $Ag^+$ concentration (0, 1, 2, 3, 4, 6, 8, 10, 20, 40, 60, 80, 100 nM). The final mixed solution was stirred and allowed to react for 15 min at 30 °C. The fluorescence spectra were measured at room temperature.

#### 2.4.3. Selectivity assays

In order to ensure the selectivity of the method towards $Ag^+$, the other 14 common metal ions and 5 common anions in natural water instead of $Ag^+$ were used to react with the above system and performed in the same manner. 200 μL of single layer $MoS_2$ solution (0.05 mg/mL) was mixed with 10 μL, 500 nM of FITC-ssDNA in 1.5 mL test tube, then the mixed solution was stirred and allowed to react for 5 min at 30 °C; after that, different metal ions (20 μL, 2 μM) in aqueous buffer were added, and finally, appropriate aliquot of PBS buffer (pH 8.00) was introduced to make each reaction solution 400 μL. The final mixed solution was stirred and allowed to react for 15 min at 30 °C. All the above experiments were conducted in PBS buffer (10 mM, 50 mM $NaNO_3$, 10 μM EDTA, pH 8.00).

#### 2.4.4. Detection of $Ag^+$ in real samples

Atomic absorption spectrometry (AAS) was applied to detect $Ag^+$ in East Lake water to verify feasibility of this new $Ag^+$ probe and obtain real concentration of $Ag^+$ in lake water. East Lake water was filtered by 0.22 μm microporous membrane.10 μL FITC-ssDNA (500 nM) was incubated with 10 μL single layer $MoS_2$ (1.0 mg/mL) for 10 min at 30 °C; later, 380 μL of East Lake water was mixed in the above solution. The final mixed solution was stirred and allowed to react for 30 min at 30 °C. Also, the detection of $Ag^+$ in tap water has been completed. 380 μL tape water was mixed with $Ag^+$ aqueous solution. Then PBS buffer was added into mixed solution and made up the final volume of 400 μL. Final $Ag^+$ concentration is (e–a) 0, 5.00, 10.00, 50.00 and 100.00 nM, respectively. And then fluorescence spectra were monitored at room temperature.

## 3. Results and discussion

### 3.1. Characterization of single layer $MoS_2$

According to the method described in literature [30] with some modifications, single layer $MoS_2$ was synthesized. To confirm the successful formation of 2D $MoS_2$ nanosheet, the as-prepared $MoS_2$ was characterized by high resolution transmission electron microscopy (HRTEM) and bulk $MoS_2$ was characterized by SEM (Fig. S1). As shown in Fig. 1A, the sheet width of single layer $MoS_2$ was approximately 10 nm exhibiting relatively narrow size distribution [34]. Raman spectrum was used to further confirm the single-layer $MoS_2$ due to line width and frequency difference of the $E^1_{2g}$ and $A_{1g}$ Raman modes, which confirmed the effective reduction of flake thicknesses from the bulk $MoS_2$ to the dispersions [21]. Results in Fig. 1B reflect the characteristics of single layer $MoS_2$. The two peaks at 384 and 409 $cm^{-1}$ are attributed to the in-plane $E^1_{2g}$ and out-of-plane $A_{1g}$ vibrations of single-layer $MoS_2$, respectively [35]. As the Raman spectra were consistent with those in previously reported literatures [18,21,32,35,36], it was proved that we had successfully prepared single layer $MoS_2$ in this work.

### 3.2. FRET between FITC-tagged ssDNA and single layer $MoS_2$

Single-layered $MoS_2$ is a kind of two-dimensional surface nanomaterial with favorable water solubility. Charge transfer from the electron donor to single or fewer layer $MoS_2$ material is substantial and is partially associated with the p-type nature of ultrathin $MoS_2$ material [37]. FITC-labeled ssDNA was absorbed rapidly when approached the surface of ultrathin $MoS_2$ via the van der Waals force between nucleobases and the basal plane of $MoS_2$, and was then quenched owing to charge transfer. Therefore, the fluorescence of FITC was efficiently quenched due to FRET between FITC and single layer $MoS_2$. According to Scheme 1, a FITC-labeled $Ag^+$ specific oligonucleotide, rich in cytosine, was employed as the fluorescent probe in sensing targets. The conformation of the probe would be changed from random coil single stranded DNA (ssDNA) to straight stiff double stranded DNA (dsDNA) with "C–$Ag^+$–C" base pairs followed by the addition of $Ag^+$. When FITC-labeled DNA probe was in the state of random coil ssDNA, FRET from FITC-ssDNA to single layer $MoS_2$ occurred, because the distance from the energy donor FITC to the energy acceptor single layer $MoS_2$ was shortened by the special p-type nature of ultrathin $MoS_2$ material [37] and Van der Waals force between nucleotide bases and single layer $MoS_2$. However, when the DNA probe was in formation of dsDNA due to the addition of $Ag^+$, the energy donor FITC was far away from the surface of single layer $MoS_2$ and FRET was disappeared. Therefore, the introduction of enough amounts of $Ag^+$ led to a large degree of fluorescence recovery, and the degree of fluorescence quenching

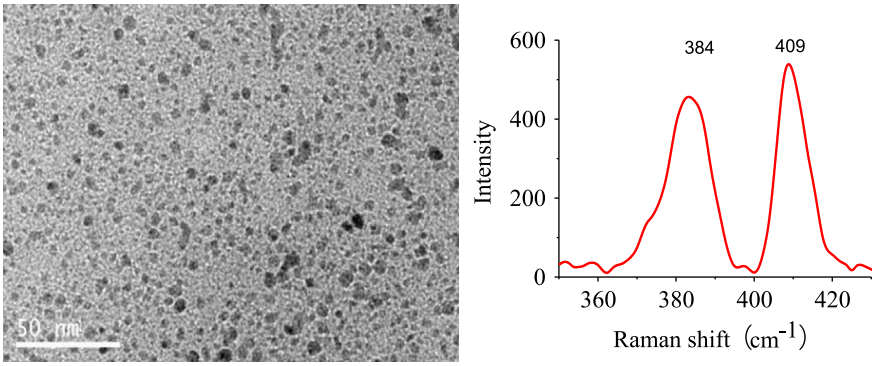


**Fig. 1.** High resolution transmission emission microscope (HRTEM) image of as-prepared single layer $MoS_2$ (A) and Raman spectra of single layer $MoS_2$ (B).

was closely related to the amount of added $Ag^+$ in certain linear range. The fluorescence of 12.5 nM FITC-ssDNA was effectively quenched by 25 μg/mL single layer $MoS_2$ (Fig. 2A, curve b), compared with the intensity without $MoS_2$ (Fig. 2A, curve a), indicating the strong quenching effect of single layer $MoS_2$ on the fluorescence of dye. The FITC-ssDNA rich in cytosine could capture $Ag^+$ by forming "C–$Ag^+$–C" base pairs. In the presence of $Ag^+$, the random coil ssDNA changed its conformation to rigid dsDNA, thus weakening the interactions between DNA nucleotide bases and single layer $MoS_2$ due to the hydrophilic force of the phosphoric skeleton in dsDNA, finally leading to the recovery of fluorescence (Fig. 2A, curve c). Results showed that the addition of $Ag^+$ induced the disappearance of FRET and the fluorescence recovery of FITC-ssDNA (Fig. 2B, curve b). Further, the fluorescence quenching kinetics was very fast, and highest fluorescence quenching efficiency was obtained within 5 min after FITC-ssDNA was mixed with the $MoS_2$ nanosheet solution. Meanwhile the fluorescence recovery kinetics was with up to best fluorescence recovery efficiency obtained within 15 min when $Ag^+$ was added into mixture solution (Fig. 3). This suggested that the designed $Ag^+$ probe system is successful and can be established with high performances.

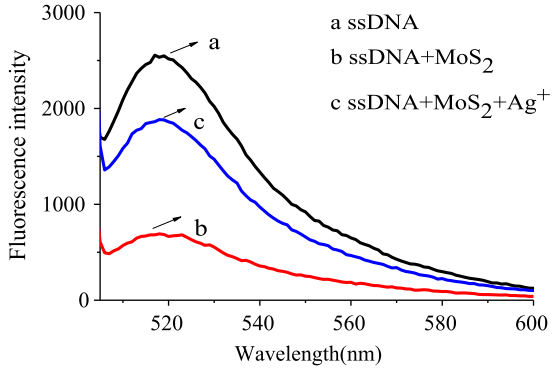


**Fig. 2.** Fluorescence spectra of before (curve a) and after (curve b) single layer $MoS_2$ (25 μg/mL) quenched 15 nM FAM-labeled ssDNA, and the change of fluorescence intensity after addition of $Ag^+$ (100 nM) (curve c). All these fluorescence spectra are carried out in PBS buffer at room temperature. The fluorescence is excited at 490 nm, and given in normalized form.

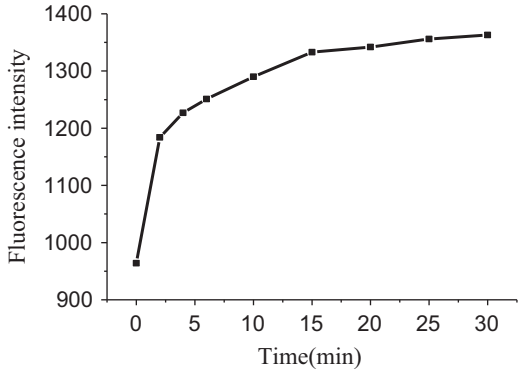


**Fig. 3.** Real-time fluorescence recovery records of mixtures with FITC-ssDNA (12.5 nM) and 25 μg/mL single layer $MoS_2$ upon additions of 100 nM $Ag^+$ (200 μL of single layer $MoS_2$ solution (0.5 mg/mL) are mixed with 10 μL 500 nM of FITC-ssDNA in cuvette, after 15 min, 20 μL of 2 μM $Ag^+$ in aqueous buffer and 170 μL PBS buffer is added. The fluorescence spectra are measured at 518 nm.).

### 3.3. Optimization of concentration of single layer $MoS_2$

Next, concentration of single layer $MoS_2$ was optimized as it is crucial in the detection of $Ag^+$ in aqueous buffer and complex water samples. As can be seen in Fig. 4A, the fluorescence intensity decreased gradually with the increasing concentration of single layer $MoS_2$, and a platform of fluorescence intensity was observed when the concentration of single layer $MoS_2$ reached 25 μg/mL (Fig. 4B). It indicated that too low concentration of single layer $MoS_2$ could lead to low fluorescence quenching efficiency and narrow detection range of $Ag^+$, while $MoS_2$ in high concentrations could have a poor effect on fluorescence recovery, and lower the sensitivity of $Ag^+$ determination. Therefore, an optimized concentration of 25 μg/mL single layer $MoS_2$ was chosen in the experiments.

### 3.4. Quantitative analysis of $Ag^+$ in aqueous buffer

As shown in Fig. 5, a new simple and sensitive assay for $Ag^+$ was successfully designed. The fluorescence intensity was dependent on the concentration of $Ag^+$ over a range of 1–100 nM when the concentration of single layer $MoS_2$ was 25 μg/mL. Fig. 5B shows that the fluorescence intensity increases rapidly as the concentration of $Ag^+$ increases from 1 nM to 6 nM ($R_1^2=0.996$). However, it exhibited another linear relationship ($R_2^2=0.995$) when the concentration of $Ag^+$ changed from 10 nM to 100 nM, where the fluorescence intensity increased more slowly as the $Ag^+$ concentration increased. The reason for this phenomenon was probably that FITC-labeled DNA in the state of random coil single strand was correspondingly abundant when $Ag^+$ was less than 6 nM in the system, and the plane structure of single layer $MoS_2$ could strongly adsorb these random coil single-strand

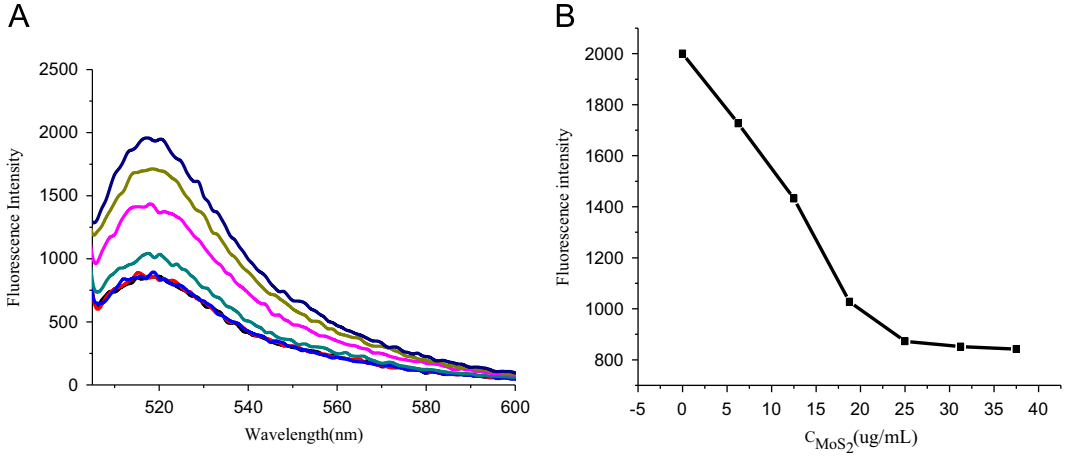


**Fig. 4.** (A) The fluorescence emission spectra of different concentrations of single layer $MoS_2$ (0, 6.25, 12.5, 18.75, 25, 31.25, 37.5 μg/mL) upon incubation with 12.5 nM FITC-ssDNA, then reacted with 100 nM $Ag^+$. (B) The fluorescence intensity at 518 nm changed against single layer $MoS_2$ concentration. The fluorescence spectra are excited at 490 nm. All experiments are in PBS buffer (10 mM, 50 mM $NaNO_3$, pH 7.4) at room temperature.

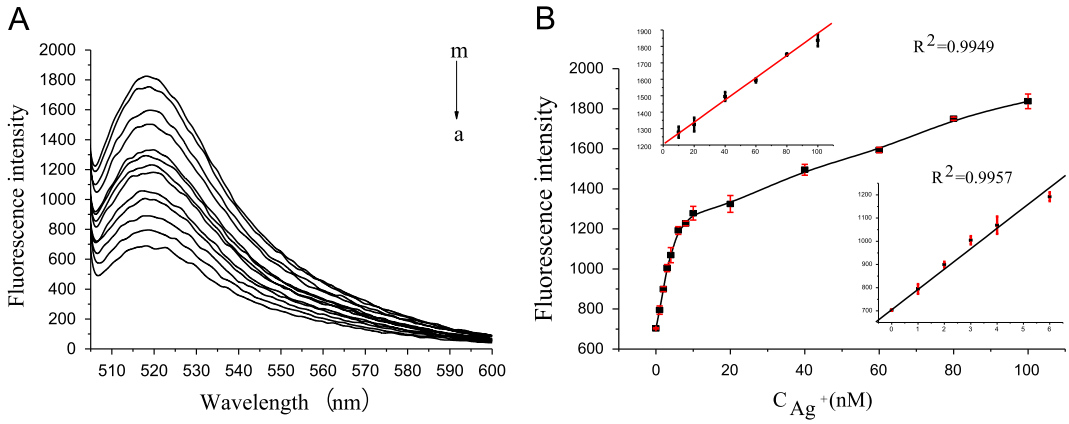


**Fig. 5.** (A) The normalized fluorescence spectra of 12.5 nM FITC-ssDNA upon incubation with 25 μg/mL single layer $MoS_2$, then reacted with a series of concentrations of $Ag^+$ (a–m: (0, 1, 2, 3, 4, 6, 8, 10, 20, 40, 60, 80, 100 nM)). (B) Calibration curve for $Ag^+$ detection in buffer, data are presented as average ± sd from three independent measurements. All these experiments are operated at room temperature and the fluorescence excitation and emission wavelengths are 490 nm and 518 nm, respectively.

**Table 1**
The precision of $Ag^+$ detection. The normalized fluorescence spectra of 12.5 nM FITC-ssDNA upon incubation with 25 μg/mL single layer $MoS_2$, then reacted with $Ag^+$ concentrations of 4.00 nM and 40.00 nM, respectively. All these experiments are operated at room temperature and the fluorescence excitation and emission wavelengths are 490 nm and 518 nm, respectively. Every experiment is repeated thrice.

| $C(Ag^+)$ (nM) | Fluorescence intensity | | | | | | | RSD(%) |
|---|---|---|---|---|---|---|---|---|
| | 0 | 6 h | 12 h | 24 h (1 d) | 2 d | 4 d | 7 d | |
| 4.00 | 1069.12 | 1072.34 | 1083.52 | 1104.64 | 1056.14 | 1047.87 | 1045.53 | 1.82 |
| 40.00 | 1495.41 | 1503.72 | 1431.35 | 1522.28 | 1436.62 | 1432.44 | 1468.36 | 2.38 |

Note: h is the abbreviation of the hour and d is the abbreviation of the day.

FITC-DNAs onto its surface, owing to the weak adsorption competition among the free FITC-ssDNA. When $Ag^+$ exceeded 6 nM in the system, free FITC-DNA in the state of random coil single strand became scarce. Adsorption competition among them became more intense, and so the fluorescence changed more slowly as the $Ag^+$ concentration increased. This method could be applied to detect as low as 1 nM (3 times the standard deviation rule) $Ag^+$ in aqueous buffer, and the detection range was wide, ranging from 1 nM to 100 nM. From this perspective, the proposed method towards $Ag^+$ has its own uniqueness, that is, the present method is much simpler and more effective to detect $Ag^+$ down to trace levels Table 1.

### 3.5. Selectivity of the method towards $Ag^+$

For determination of $Ag^+$ in natural water, the main interference includes other metal ions, such as $Ca^{2+}$ and $Mg^{2+}$, because they always coexist with $Ag^+$. The results are demonstrated in Fig. 6, showing that no other metal ions interfered with the detection of $Ag^+$ in natural water. Furthermore, the effects of the other 12 common metal ions were taken into account. Typically, under optimum experimental conditions, the $Ag^+$ detection system was incubated respectively with 100 nM $Ag^+$ and 10 μM other 12 other metal ions in PBS buffer. As shown in Fig. 6, compared with the $Ag^+$ system, the existence of the other 12 commonly seen metal ions had almost no influence on detection of $Ag^+$. This suggested that the binding affinity of $Ag^+$ to a "C–C" mismatch site appeared to be much stronger than that to all metal ions except for $Ag^+$. The results clearly illustrated the specificity of the method for $Ag^+$.

### 3.6. Detection of $Ag^+$ in real samples

In order to further investigate the potential application of the sensor in the practical samples, the assay was used to detect $Ag^+$ in lake water and tap water. The concentration of $Ag^+$ in lake water

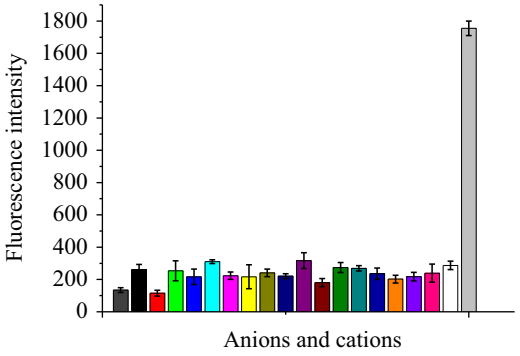


**Fig. 6.** Selectivity of single layer $MoS_2$-based method for Ag+. The other 14 common metal ions and 5 common anions in natural water instead of $Ag^+$ are used to react with above system and performed in the same way. The $Ag^+$ concentration of 100 nM is tested, while the concentration of other inspected species is 10 μM. All these experiments are operated at room temperature and the fluorescence excitation and emission wavelengths are 490 nm and 518 nm, respectively. Note: from left to right: $Cl^-$, $SO_4^{2-}$, $NO_3^-$, $PO_4^{3-}$, $HCO_3^-$, $Ni^{2+}$, $Cu^{2+}$, $Cr^{3+}$, $K^+$, $Na^+$, $Fe^{3+}$, $Pb^{2+}$, $Co^{2+}$, $Mn^{2+}$, $Hg^{2+}$,$Zn^{2+}$, $Al^{3+}$, $Fe^{2+}$, $Mg^{2+}$ and $Ag^+$.

from the East Lake of Wuhan, Hubei Province, China was chosen to detect $Ag^+$. To verify the feasibility of this new $Ag^+$ probe and obtain real concentration of $Ag^+$ in lake water, atomic absorption spectrometry (AAS) was applied to verify $Ag^+$ concentration in East Lake water compared with the $Ag^+$ probe in this work. Real concentration of $Ag^+$ detected by AAS in lake water is 1.039 nM ($SD$=0.002, $n$=3). As shown in Fig. 7, the concentration of detection of $Ag^+$ in the lake water (Fig. 7, curve b) was approximately equal to 1.04 nM $Ag^+$ in aqueous buffer (Fig. 7, curve a). It is probably that lake water contained many kinds of metal ions. These complicated materials in lake water could stabilize the fluorescence strength in some way and on the other hand, they might also participate in the nonspecific adsorption competition with each other onto the single

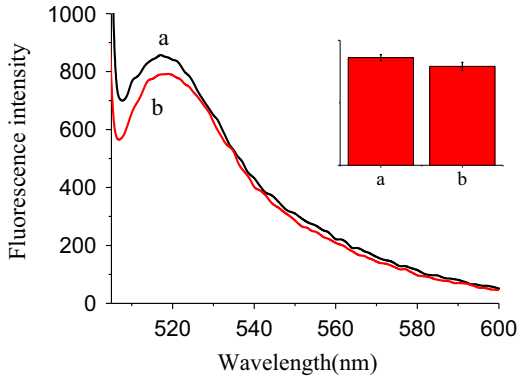


**Fig. 7.** Detection of $Ag^+$ in the East Lake water samples using fluorescence spectra of (a) single layer $MoS_2$+FITC-ssDNA+1 nm$Ag^+$ aqueous buffer (b) single layer $MoS_2$+FITC-ssDNA+ lake water. Inset: corresponding histograms with error bar (standard deviation from the mean, $n=3$). Excitation wavelength is at 490 nm, and the emission intensity is monitored at 518 nm.

**Table 2**
Rate of recovery of $Ag^+$ 0.380 μL lake water mixed with $Ag^+$ aqueous solution, mixed solution final volume is 400 μL and final $Ag^+$ concentration are 4.00,8.00 and 12.00 nM, respectively. All these experiments are operated at room temperature and the fluorescence excitation and emission wavelengths are 490 nm and 518 nm, respectively.

| Addition concentration of $Ag^+$ (nM) | Measured concentration of $Ag^+$ (nM) | | | | Rate of standard addition recovery (%) | | | |
|---|---|---|---|---|---|---|---|---|
| – | $n=1$ | $n=2$ | $n=3$ | Average | $n=1$ | $n=2$ | $n=3$ | Average |
| 0 | 1.02 | 0.98 | 1.04 | 1.01 | – | – | – | – |
| 4.00 | 4.64 | 4.62 | 4.73 | 4.66 | 90.75 | 90.25 | 93.00 | 91.33 |
| 8.00 | 8.75 | 8.31 | 8.64 | 8.57 | 96.75 | 91.25 | 95.38 | 94.46 |
| 12.00 | 12.36 | 12.44 | 12.71 | 12.50 | 94.58 | 95.25 | 97.50 | 95.78 |

layer $MoS_2$ surface. All these reasons led to the comprehensive result. Meanwhile, standard addition recovery experiment has been completed in our work. FromTable 2, good result (more than 90%) for rate of recovery of $Ag^+$ was obtained. Also, we have show an application of the proposed method in the tap water. According to our experimental data, no $Ag^+$ can be detected in tap water. So, low and certain concentrations of $Ag^+$ have been spiked into tap water. The result we detected for the concentrations of $Ag^+$ is closed to the theoretical concentration (see Fig. S2 in the Supporting information). In addition, the toxic levels for $Ag^+$ in drinking water are defined by the United States Environmental Protection Agency (USEPA) to be 10 nM [38]. The detection limit of this assay for $Ag^+$ (1 nM) was lower than the maximum limitation guided by the United States Environmental Protection Agency (EPA) as well as that permitted by the World Health Organization (WHO). Therefore, this sensor demonstrated great potential in practical applications.

## 4. Conclusion

In summary, a simple and novel approach based on FRET between single layer $MoS_2$ and FITC-ssDNA for detection of $Ag^+$ was proposed for the first time in this work. The proposed method exhibits higher sensitivity and selectivity toward $Ag^+$ even in the presence of other competitive heavy metal ions. Importantly, $Ag^+$ ion detections in lake water samples are performed to demonstrate the capablility of the sensor in practical applications. The developed sensor with high sensitivity and selectivity may be an alternative method for $Ag^+$ ion detection in environmental, biomedical, and other applications. Furthermore, we expect that this strategy based on single layer $MoS_2$ as fluorescent quencher may offer a new approach in sensitive and selective detection of a wide spectrum of analytes, high-through put drug screening and other metal ions.

## Acknowledgments

We gratefully acknowledge the support from the Natural Science Foundation of China (NSFC) (Nos. 20927003, 90913013, 41273093 and 21175101), the National Major Scientific Instruments and Device Development Project (2012YQ16000701), and the Foundation of China Geological Survey (Grant no. 12120113015200).

## Appendix A. Supporting information

Supplementary data associated with this article can be found in the online version at http://dx.doi.org/10.1016/j.talanta.2014.10.026.

## References

[1] V.P. Hiriart-Baer, et al., Aquat. Toxicol. 78 (2006) 136–148.
[2] J.R. Shaw, et al., Environ. Toxicol. Chem. 17 (1998) 594–600.
[3] M.N. Croteau, et al., Environ. Sci. Technol. 45 (2011) 6600–6607.
[4] Y. Yang, et al., Anal. Biochem. (2012) 48–52.
[5] W. Pu, et al., Microchim. Acta 177 (2012) 137–144.
[6] C.X. Tang, et al., Chem. Commun. 47 (2011) 12304–12306.
[7] A. Porchetta, et al., J. Am. Chem. Soc. 135 (2013) 13238–13241.
[8] C.Y. Lin, et al., Anal. Chem. 82 (2010) 6830–6837.
[9] C. Zhao, et al., Chem. Eur. J. 16 (2010) 8147–8154.
[10] I.T. Ho, K.C. Haung, W.S. Chung, Chem.– Asian J. 6 (2011) 2738.
[11] L. Liu, et al., Org. Lett. 10 (2008) 2271–2274.
[12] X. Zhu, et al., Tetrahedron Lett. 49 (2008) 1843–1846.
[13] K.M.K. Swamy, et al., Chem. Commun. (2009) 1234–1236.
[14] L. Liu, et al., Org. Lett. 10 (2008) 4581–4584.
[15] F. Wang, et al., Inorg. Chem. 50 (2011) 2240–2245.
[16] A. Chatterjee, et al., J. Am. Chem. Soc. 131 (2009) 2040–2041.
[17] M. Aliofkhazraei, N. Ali, Two-Dimensional Nanostructures, CRC Press, Boca Raton, FL, USA, 2012.
[18] S.Z. Butler, et al., ACS Nano 7 (2013) 2898–2926.
[19] D. Yang, et al., Phys. Rev. B 43 (1991) 12053–12056.
[20] M. Buscema, et al., Nano Lett. 13 (2013) 358–363.
[21] K. Wang, et al., ACS Nano 7 (2013) 9260–9267.
[22] Q.H. Wang, et al., Nat. nanotechnol. 7 (2012) 699–712.
[23] T. Wang, et al., Anal. Chem. 85 (2013) 10289–10295.
[24] C. Zhu, et al., J. Am. Chem. Soc. 135 (2013) 5998–6001.
[25] N. Goswami, A. Giri, S.K. Pal, Langmuir 29 (2013) 11471–11478.
[26] G.H. Clever, C. Kaul, T. Carell, Angew. Chem. Int. Ed. 46 (2007) 6226–6236.
[27] Y. Tanaka, et al., J. Am. Chem. Soc. 129 (2007) 244–245.
[28] D. Huang, et al., Environ. Sci. Technol. 47 (2013) 4392–4398.
[29] Z. Lin, X. Li, H.B. Kraatz, Anal. Chem. 83 (2011) 6896–6901.
[30] P. Joensen, et al., Mater. Res. Bull. 21 (1986) 457–461.
[31] Z. Zeng, et al., Angew. Chem. Int. Ed. 50 (2011) 11093–11097.
[32] V. Nicolosi, et al., Science 340 (2013) 1226419.
[33] Z. Zeng, et al., Angew. Chem. Int. Ed. 51 (2012) 9052–9056.
[34] S. Ji, et al., Electrochim. Acta 109 (2013) 269–275.
[35] Z. Yin, et al., ACS Nano 6 (2011) 74–80.
[36] H. Li, et al., Small 8 (2012) 682–686.
[37] S. Dey, et al., Chem. Asian J. (2013) 1780–1784.
[38] T. Li, et al., Chem. Eur. J. 15 (2009) 3347–3350.